MAX-PLANCK-INSTITUT FÜR PLASMAPHYSIK

GARCHING BEI MÜNCHEN

STOCHASTIC HEATING OF PLASMA ELECTRONS USING MICROWAVE NOISE

S. Puri

IPP IV/57 June 1973

Die nachstehende Arbeit wurde im Rahmen des Vertrages zwischen dem Max-Planck-Institut für Plasmaphysik und der Europäischen Atomgemeinschaft über die Zusammenarbeit auf dem Gebiete der Plasmaphysik durchgeführt.

IPP IV/57 S. Puri

Stochastic Heating of Plasma Electrons using Microwave Noise

June 1973 (in English)

Abstract

A mirror-contained hydrogen plasma of approximately 1 liter volume, 1 x 10^{11} cm^{-3} density and 1 keV temperature is produced using 100 watt broadband microwave noise at the electron cyclotron resonance. In contrast to the single frequency heating, noise heating is stable, repeatable and more efficient. The use of Ioffe bars is found to be indispensable in suppressing the low-frequency instabilities and the attendant plasma loss, as well as for assuring reproducibility. Detailed measurements of the density, diamagnetic and energy analyzer measurements are presented for several values of power input, noise bandwidth and gas pressure. Independent measurements of density and diamagnetic signal decay in the afterglow plasma are also given.

1. INTRODUCTION

Stochastic acceleration has been proposed as a possible mechanism for the production of energetic particles in the cosmic rays (FERMI, 1949), bow shock (FAN et al., 1964), beam-plasma interactions (STIX, 1964) as well as for the heating of mirror-contained plasmas in the laboratory by the application of external electromagnetic fields (SEIDL, 1964; LICHTENBERG et al., 1969; GRAWE, 1969; KAWAMURA et al. , 1972; LIEBERMAN and LICHTENBERG, 1973). In a more general sense, stochastic acceleration plays an important role in the absorption and randomization of energy under all turbulent conditions whether produced by strong applied electric fields (HAMBERGER, 1970) or induced by impulsive currents (WHARTON et al., 1971).

Due to the complexity of the problem, a self consistent solution is rarely attempted. The more common approach is to study the motion of a test-particle in a specified electromagnetic field. The stochasticity may occur through virtual collisions due to phase randomization occuring in regions of magnetic field inhomogeneities e.g. reflection in a magnetic mirror (SMULLIN, 1965). In this paper, however, further discussion will be restricted to the case where the stochasticity is an inherent property of the electromagnetic field itself. In either case, the pertinent quantity determining the acceleration rate and the evolution of the particle energy distribution function is the actual field at the particle´s instantaneous

position. For a particle situated in a uniform, static magnetic field, the acceleration rate can be uniquely specified in-terms-of the correlation spectra, provided that the fluctuating field as seen by the particle is "weak" and "stationary" in the statistical sense (SHAPIRO, 1965; BASS et al., 1966; STURROCK, 1966; PURI, 1966; BOL, 1966; HALL and STURROCK, 1967).

Since, a plasma in order to be heated must be contained (e.g. in a magnetic mirror) before the stochastic heating theories can be experimentally verified, the treatment must be extended to allow for spatial non-uniformities in the static magnetic field. Such an extension is possible (PURI, 1968) provided that the transverse experimental dimensions are small compared to the free-space wavelength of the applied rf field and the bounce frequency of the particle in the mirror is small in comparison with the rf field frequency.

We have previously reported an experiment (PURI et al. 1968) in which the above theoretical predictions were verified by heating a low density (10^7 cm^{-3}), mirror-contained sodium plasma from 0.2 to 0.4 eV by coupling approximately 1 μwatt of rf noise at the electron gyrofrequencies in the mirror.

In the experiment to be described in this paper the primary objective is a more convincing demonstration of electron heating to high temperatures using 100 watt broadband rf power rather than a detailed comparison with the theory. Since the typical collision mean-free-path is several hundred times the apparatus dimensions and the collision frequency much smaller than the noise bandwidth, genuine stochastic heating rather than collisional heating may be expected to dominate. Density and tem-

perature measurements for several values of power input, noise bandwidth and gas pressure are presented. The repeatable, stable plasma produced by noise heating facilitates study of mirror containment properties and in particular, unequivocally confirms the importance of a minimum magnetic field configuration.

2. BRIEF REVIEW OF THE THEORY

A charged particle in a stochastic electric field executes a random walk in velocity space and consequently is accelerated. This result is readily derived from the equation of motion

$$v(t) = v(o) + \int_o^t \frac{q}{m} E(t)\, dt \qquad (1)$$

where $E(t)$ is the electric field component parallel to the particle velocity. If $E(t)$ is stationary random, the incremental velocity has an equal probability of acquiring either a positive or a negative value with a prescribed magnitude. Hence $\langle v(t) \rangle$, the expected value of the velocity remains unchanged equal to $v(o)$; but $\langle v^2(t) \rangle$ increases so that the particle gains energy.

Alternatively, consider a segment of a stochastic electric field at the particle gyrofrequency (a stochastic field may be regarded as compared of segments of a sinusoidal field dephased at random intervals) applied to a charged particle in the direction transverse to the static magnetic field. The particle undergoes either acceleration and spirals outwards or it suffers deceleration and spirals inwards depending upon its relative phase φ with respect to the electric field. The force on the particle is $qE \cos \varphi$ and its energy change is given by the

product of this force with the distance moved,

$$\Delta\mathcal{E} = qE \cos\varphi \ \Delta S \qquad (2)$$

Assuming that can equally likely have any value between 0 and 2π, it is at once clear that on probability bases there is net energy imparted to the particle because ΔS for an accelerated particle is greater than that for a decelerated particle. If the electric field is switched on repeatedly but each time with a randomly shifted phase, the particle will continually extract energy from the field. The precise expression for the acceleration rate for this case may be written in-terms-of the spectrum functions as

$$d\langle v^2\rangle /dt = 2\pi \ (q/m)^2 \ \bar{\Phi} \quad (\omega_c) \qquad (3)$$

where $\bar{\Phi}\ (\omega_c)$ is the power spectrum at the cyclotron frequency of the random electric field <u>as seen by the particle</u>. The bulk of the theoretical effort has been directed towards the evaluation of $\bar{\Phi}\ (\omega_c)$, allowing the electric field to have an arbitrary spectrum in frequency and wave number (STURROCK, 1966) and eventually allowing for the finite gyroradius effects (HALL and STURROCK, 1967) which introduce cyclotron-harmonic interaction in addition to the gyroresonance. As was pointed out in the introduction, for the special case of spatially uniform electric field, the above treatment may be extended (PURI, 1968) to allow for a static mirror magnetic field.

Some of the unfortunate restrictions in these theories include the neglect of interparticle interactions, the assumptions of statistical independence among the particles as well

as the limitation to electrostatic turbulence (PURI, 1973). As a result an experimental comparison, except for the very simple case already described in the introduction, is generally not feasible. Nevertheless, whenever pertinent, the general features of the theory reflected in the experimental observations will be pointed out. Note that all temperature values refer to the plasma kinetic temperature.

3. DESCRIPTION OF THE EXPERIMENT.

Part of a 6 cm diameter quartz tube is enclosed in a multimode copper cavity 39 cm long and 15 cm in diameter as shown in Fig. 1. Gas is admitted into the tube at one end while the other end is evacuated by a turbomolecular pump. An extremely clean vacuum is obtained through the use of hard silver brazing, all metal flange seals and hot air baking resulting in a base pressure of less than 1×10^{-8} Torr. Such cleaning is found to be crucial for obtaining high electron temperatures and for experimental reproducibility over a period of a year. Another factor contributing towards repeatability is the accurate control of the gas feed. The gas pressure is monitored continuously with a Penning gauge whose operation is immune to the static magnetic field switching. The output signal from the Penning gauge is used for regulating the pressure in conjunction with an automatic pressure controller.

A 34-cm-long magnetic mirror with the field strength varying between 3 kG in the middle and 4.5 kG at the ends is used for plasma confinement. The curvature of the mirror field gives rise to an effective negative well in the transverse direction. The

transverse well depth varies along the length of the mirror reaching a maximum magnitude of -1.7%. A set of four Ioffe bars can produce a minimum magnetic field with a transverse well depth of upto + 2.5% which would not only be sufficient to offset the negative well depth occuring in the mirror but could also produce a substantial effective positive well depth for the stabilization of interchange instabilities.

Plasma formation and electron heating are accomplished by feeding 100 watt broadband (8 - 12 GHz, corresponding to the electron cyclotron frequencies in the mirror) microwave power with the spectrum shown in Fig. 2. The microwave power is derived by amplification of noise from a gas discharge tube using travelling wave amplifiers (TWA's). After division into two equal parts using a 3 db coupler, the microwave power is coupled into the plasma at the two ends with microwave horns. Of the 100 watt amplifier output approximately 20 watt power is lost in circulators, waveguides or through reflections while 80 watt is radiated from the horns.

The principal diagnostics have been performed with an 8-mm microwave interferometer, a movable diamagnetic coil and an electrostatic electron energy analyzer. Additional measurements planned with a cylindrical (2 mm long, 0.01 mm diameter) Langmuir probe were not possible due to probe burnout. Also, a spherical (1 mm diameter) Langmuir probe proved to be unusable owing to excessive perturbation of the plasma.

The microwave interferometer is temperature compensated and the phase shift is directly read off a polar display. The reading accuracy of 1^{o} in the pulsed mode corresponds to an accuracy of 1×10^{10} cm^{-3} in the density measurements.

The plasma diamagnetic pressure is measured using a modified version of the method devised by LEVINE and KUCKES (1967). The probe consists of two copper coils (Fig. 3) of 100 and 20 turns respectively, electrostatically shielded from each other and enclosed in a thin stainless steel casing with a small air gap in the azimuthal direction. In order to calibrate the probe, current pulses of known shape and magnitude are passed alternately through the 20-turn coil and through a solenoid (of the dimensions of the plasma) placed inside the quartz tube. On integrating the signal from the 100-turn coil, the original pulses are recovered. Since the calibration is conducted with the copper cavity in place, this procedure allows the calibration of the diamagnetic signal independent of the eddy current losses. Furthermore, the calibration is insensitive to electronic signal processing and we retain the freedom to use whatever amplification or filtering deemed necessary for the optimum recovery of the signal in the presence of plasma noise and magnetic field disturbances. In fact in subsequent experiments, it is necessary to remove the low-frequency pickup due to the confining field ripple using a combination of high-pass filters, amplifiers and averaging the results of several thousand shots using a signal analyzer.

The electrostatic energy analyzer (Fig. 1) measures the energy distribution of the electrons escaping through the mirror loss cone. After admitting the particle beam into the energy analyzer through a 3 mm diameter graphite aperture, the ions are repelled back by the positively biased cylindrical

(5 mm inner diameter, 25 mm long) drift tube A. The variable negative bias on tube B selects the electrons for admission into the graphite collector and the collector current (typically 1 μa) is measured across 1 MΩ resistor. The grounded drift tube C discourages an avalanche buildup due to the returning secondaries emitted from the collector. The secondary emission is itself suppressed through the use of graphite for the collector and zirconium for the drift tube construction. To offset the effect of outgassing from the graphite, which could seriously undermine the accuracy of the measurements, the energy analyzer is independently evacuated by a second turbomolecular pump. The entire energy analyzer is embedded in a strong magnetic field (approximately 3 kG) in order to prevent the divergence of the electron beam to the drift tubes.

4. THE EXPERIMENTAL RESULTS

4.1 Plasma reproducibility

Besides being obviously desirable, plasma reproducibility is crucial for diamagnetic pressure measurements which are typically averaged over several thousand shots in order to retrieve the signal masked by the low-frequency noise due to magnetic field fluctuations. The three most important means for realizing this objective include:

(i) A clean vacuum with a base pressure below 1×10^{-8} Torr is obtained through the combination of strong pumping,

quartz, stainless steel and OHFC copper, hard brazed construction, hot air baking and finally microwave pulse cleaning. The adverse effect of the impurities is apparent after system airing. In measurements performed when the base pressure is 1×10^{-6} Torr, the electron temperature would not exceed 100 eV whereas for identical parameters in the cleaned system electron temperatures of typically 1 keV are obtained.

(ii) As mentioned in Sec. 3, continuous feedback regulation of the input gas pressure is also essential for ascertaining repeatability.

(iii) By far the most dramatic contribution to repeatability is made by the introduction of a quadrupole magnetic field (transverse to the mirror field) using a set of four Ioffe bars. Although each of the Ioffe bars is capable of conducting 48,000 amperes; in normal operation 16,000 amperes are found to be adequate for stabilizing the low-frequency density fluctuations and the attendant plasma loss. The transverse well depth of about + 0.8% superposed on the negative well depth arising from the curvature of the mirror field is presumably sufficient to produce an average minimum magnetic field along the particle trajectories. Figure 4 shows some typical density signals without (middle) and with (bottom) the energization of the Ioffe bars. The top trace corresponds to the 100 watt microwave noise heating pulse fed into the plasma for four different values of the gas pressure. The stabilizing effect assumes increasing prominence as the gas pressure is lowered. For pressures below 3×10^{-5} Torr

and down to 4 x 10^{-6} Torr ignition is possible only if the Ioffe bar field is applied.

4.2 Role of noise bandwidth

The electron cyclotron frequencies corresponding to the magnetic field (3 - 4.5 kG) in the mirror roughly span the x-band microwave frequencies between 8 and 12 GHz. By inserting suitable low- and high-pass filters at the input of the microwave power amplifier it is possible to select variable noise bandwidths of 4 GHz (8 - 12 GHz), 3 GHz (9 - 12 GHz), 2 GHz (9.5 - 11.5 GHz), 1 GHz (10 - 11 GHz) or 0.5 GHz (10 - 10.5 GHz) while a fixed power output of 100 watt is maintained by adjusting the variable attenuator between the pre- and power amplifier.

Figure 5 shows the plasma density and electron temperature obtained at a fixed gas pressure of 1 x 10^{-5} Torr as the noise bandwidth is varied between 0.5 GHz and 4 GHz. While the density decreases monotonically albeit slowly with increasing bandwidth, the temperature displays a slight maxima for the 3 GHz bandwidth. The overall effect of bandwidth changes may be characterized as being mild. The reasons for this behaviour will be discussed presently.

At this juncture it would be appropriate to compare broadband heating with simular measurements conducted with single frequency heating. This is readily accomplished by replacing the gas discharge noise source by a x-band microwave signal generator. It is found that no plasma can be produced using

signal frequencies either below 9 GHz or above 12 GHz, which would establish that the cyclotron interaction is indeed responsible for the electron heating. Using the most optimum frequency of 10.5 GHz, electron temperatures of about 100 eV are obtained which nevertheless compares unfavourably with 1 keV temperature plasmas produced using broadband heating. Even at this optimum frequency no plasmas could be produced with less than 70 watt input, whereas with noise heating ignition is possible with as little as 10 watt input (see Sec. 4.3). Furthermore, the heating is extremely sensitive to slight alterations in the magnetic field as well as to changes in the heating frequency in contrast with noise heating which is insensitive to small changes in the magnetic field or the spectrum bandwidth. These observations support the theoretical results (PURI, 1968) which predict the plausibility of efficient heating with a narrow band source provided that the heating frequency is adjusted to maximize the absorption efficiency which may be a delicate function of the exact mirror configuration as well as the particle energy. Since the noise bandwidth always included the frequency regime of efficient energy transfer, in the results quoted in the previous paragraph, the heating was relatively insensitive to the changes in the spectrum bandwidth.

4.3 Changes in input power and gas pressure

Density and temperature measurements using noise bandwidth of 0.5 GHz will now be described. Figure 6 shows interferometer

(polar display, left) and diamagnetic signals (flat topped signals on the right) for input power ranging between 10 W and 100 W. The diamagnetic pressure can be directly calculated from the triangular calibration signals whose height corresponds to the value $10^{13} cm^{-3}$ eV. The calculated values of density and temperature are plotted in Fig. 7 as a function of the microwave input power. Initial increase in power gives rise to higher densities while subsequent increases contribute principally to temperature increases.

Independent estimate of the electron temperature is obtained (Fig. 7) from the electron energy analyzer described in Sec. 3. Since the collision mean-free-path is much larger than the apparatus dimensions, the probability of particle scattering into the loss cone varies approximately as $\mathcal{E}^{-3/2}$. Inclusion of this correction in the energy analyzer measurements results in an agreement with the diamagnetic temperature within $\pm$ 50%. This might be considered satisfactory considering the possibility of inaccuracies arising from the somewhat involved interpretation of the energy analyzer data. The particle energy distribution for an input noise power of 100 watt is shown in Fig. 8 (solid curve) and is seen to be in considerable variance with the Maxwell-Boltzmann distribution shown by the dashed curve.

The increasing gas pressure (keeping a fixed 100 watt power input) has the predictable effect of increased density and decreased electron temperature as shown in Fig. 9. The degree of ionization is typically 10%. At gas pressures below

$\sim$ 3 x 10^{-5} Torr strong X-ray emission is observed. The emission intensity is peaked near the microwave horn away from the gas inlet and nearest to the pump (see Fig. 1). The measured intensity just outside the middle of the copper cavity at 1 x 10^{-5} Torr pressure and 100 watt noise heating power is approximately 2.5 Röntgen/hour with an energy of 120 keV and could presumably be produced by high energy electrons penetrating deep into the mirror throats and subjected to intense microwave heating for a relatively prolonged duration. The X-ray radiation necessitated the surrounding of the experiment with 6-mm lead plating.

4.4 Density and diamagnetism decay

Fig. 10 shows the buildup and decay of the diamagnetic (lower left) and density (upper right) signals for several values of the gas pressure. The microwave heating pulse of 500 μsec duration is also shown (upper left and lower right). Whilst the density falls off slower as the pressure is lowered, the characteristic energy decay time of about 150 μsec is practically independent of the gas pressure as seen in Fig. 9.

A simple energy balance calculation using energy containment time of 150 μsec shows that typically over 50% (40 watt of the possible 80 watt radiated from the microwave horns) of the available microwave power is coupled into the plasma.

5. DISCUSSION

Beyond experimentally confirming the hitherto largely theoretical predictions of the possibility of plasma heating

using random electromagnetic fields, the superior performance of noise heating compared to single frequency heating in a magnetic mirror has been clearly demonstrated.

Also, the effectiveness of minimum magnetic field configuration for suppressing plasma instabilities and the correlation of these instabilities with plasma loss is apparent from the higher plasma temperatures obtained when the Ioffe bars are energized.

Although the relatively high expense of generating even moderate anrounts of noise power may relegate this approach for plasma heating to merely academic interest, the method could nevertheless be used if hot, stable and highly reproducible plasmas were required for precise measurements.

ACKNOWLEDGEMENT

I express my gratitude to Mr. Jochen Ernesti who was responsible for the design, construction and the operation of the experiment. In addition, the help of Mr. Helmut Rebischki for the glass constructions, of Dr. Manfred Tutter for the initial design considerations, and of Dr. Tutter and Mr. Otto Gehre for the construction of the microwave interferometer is appreciated.

REFERENCES

BASS, F.G., FAINBERG, Ya.B. and SHAPIRO, V.D. (1966)
Sov. Phys. JETP 22, 230.

FAN, C.Y.,GLOEKLER, G. and SIMPSON, J.A. (1964)
Phys. Rev. Letters 13, 149.

FERMI, E. (1949) Phys. Rev. 75, 1169.

GRAWE, H. (1969) Plasma Physics 11, 151.

HALL, D.E. and STURROCK, P.A. (1967) Phys. Fluids 10, 2620.

HAMBERGER, S.M. and JANACARIK, J. (1970)
Phys. Rev. Letters 25, 999.

KAWAMURA, T., NAMBA, C. and TERASHIMA, Y. (1973)
Symposium on Plasma Heating and Injection, International School of Plasma Physics, Varenna, Italy, p. 244.

LEVINE, A.M, KUCKES, A.F. and MUTLEY, A.W. (1967)
J. Appl. Phys. 38, 4435.

LICHTENBERG, A.J., SCHWARZ, M.J. and TUMA, D.T. (1969)
Plasma Physics 11, 101.

LIEBERMAN, M.A. and LICHTENBERG, A.J. (1973)
Plasma Physics 15, 125.

PURI, S. (1966) Phys. Fluids 9, 1043 and 2043.

PURI, S. (1968) Phys. Fluids 11, 1745.

PURI, S., DUNN, D.A. and THOMASSEN, K.I. (1968)
Phys. Fluids 11, 2728.

PURI, S., (1973), Symposium on Plasma Heating and Injection, International School of Plasma Physics, Varenna, Italy, p. 197; Report IPP IV/44, Max-Planck-Institut für Plasmaphysik, D-8046 Garching, West Germany (1972).

SEIDL, M. (1964) J. Nucl. Energy Pt. C6, 597.

SHAPIRO, V.D. (1965) JETP Letters 2, 291.

SMULLIN, L.D. (1965) Phys. Fluids 8, 1412.

STIX, T.H. (1964) Phys. Fluids 7, 1690.

STURROCK, P.A. (1966) Phys. Rev. 141, 186.

WHARTON, C.B., KORN, P., and ROBERTSON, S. (1971)
Phys. Rev. Letters 27, 499.

FIGURE CAPTIONS

Fig. 1 Schematic of the experiment

Fig. 2 Microwave noise spectrum

Fig. 3 Diamagnetic probe calibration

Fig. 4 Plasma density signal from the 8-mm interferometer without (middle trace) and with (bottom trace) the Ioffe bar current for several values of gas pressure and 100 watt input noise power. The upper trace shows the duration of the heating pulse.

Fig. 5 Plasma density and electron temperature as a function of the noise bandwidth.

Fig. 6 Plasma density (polar trace, left) and diamagnetic signals (flat topped signal, right) for several values of input power with the fixed gas pressure of 3×10^{-5} Torr and 0.5 GHz (10 - 10.5 GHz) noise bandwidth. The triangular signal is the diamagnetic pressure calibration signal.

Fig. 7 Plasma density and electron temperature versus input power calculated from the data in Fig. 6.

Fig. 8 Electron energy distribution measured with the electrostatic electron-energy-analyzer for the parameters of Fig. 6 using 100 watt input noise power.

Fig. 9 Density and temperature as well as the characteristic plasma and diamagnetism decay times versus gas pressure for an input noise power of 100 watt and spectrum width from 10 - 10.5 GHz.

Fig. 10 Buildup and decay of diamagnetic pressure (lower left) and plasma density (upper right) for several values of the gas pressure. The duration of the 500 µsec, 100 watt noise heating pulses is shown by the traces on upper left and lower right.

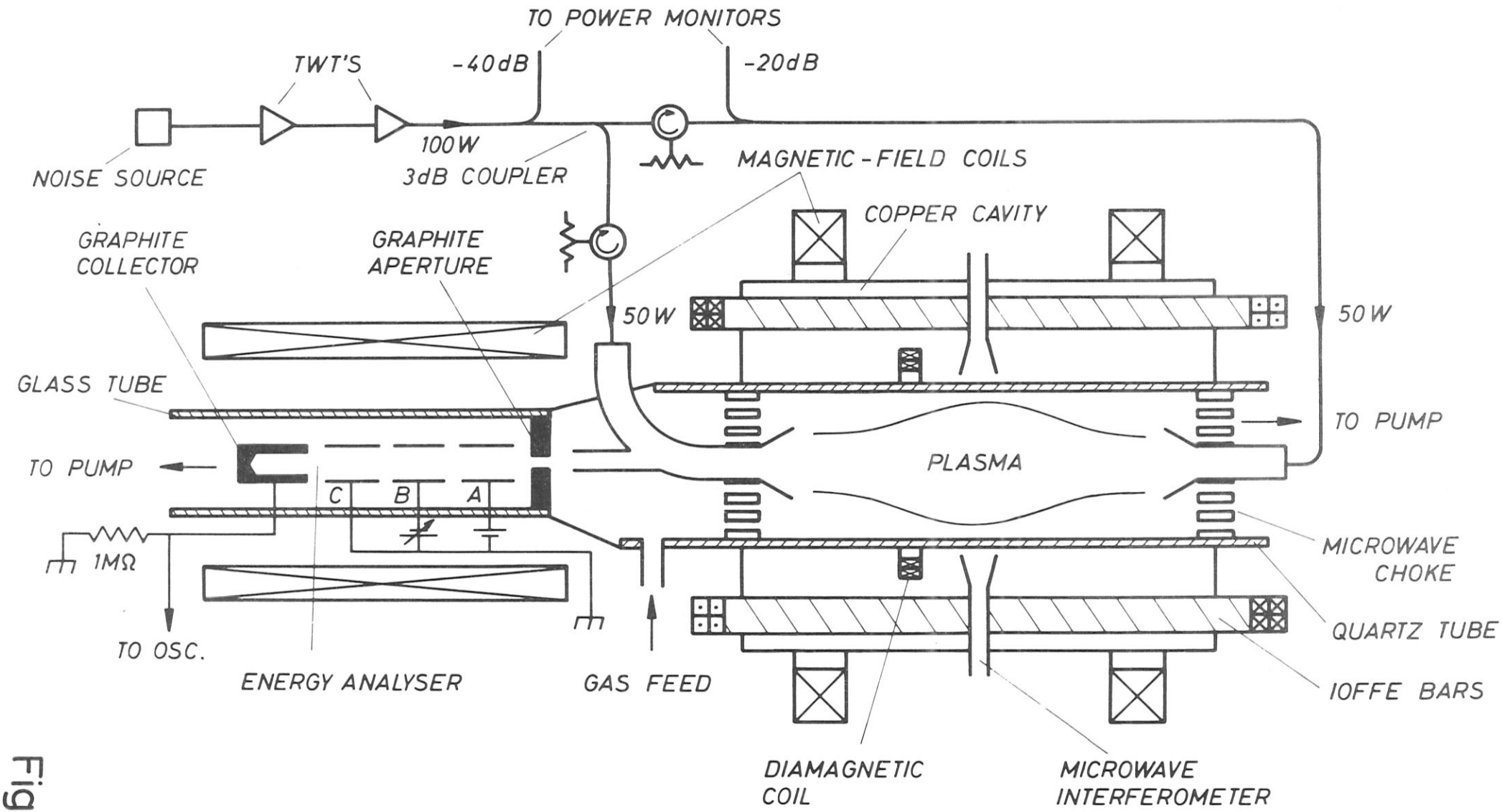
TO POWER MONITORS
TWT'S
-40dB
-20dB
NOISE SOURCE
100W
3dB COUPLER
MAGNETIC-FIELD COILS
COPPER CAVITY
GRAPHITE COLLECTOR
GRAPHITE APERTURE
50W
50W
GLASS TUBE
TO PUMP
TO PUMP
PLASMA
C
B
A
1MΩ
MICROWAVE CHOKE
QUARTZ TUBE
TO OSC.
ENERGY ANALYSER
GAS FEED
IOFFE BARS
DIAMAGNETIC COIL
MICROWAVE INTERFEROMETER

Fig. 1

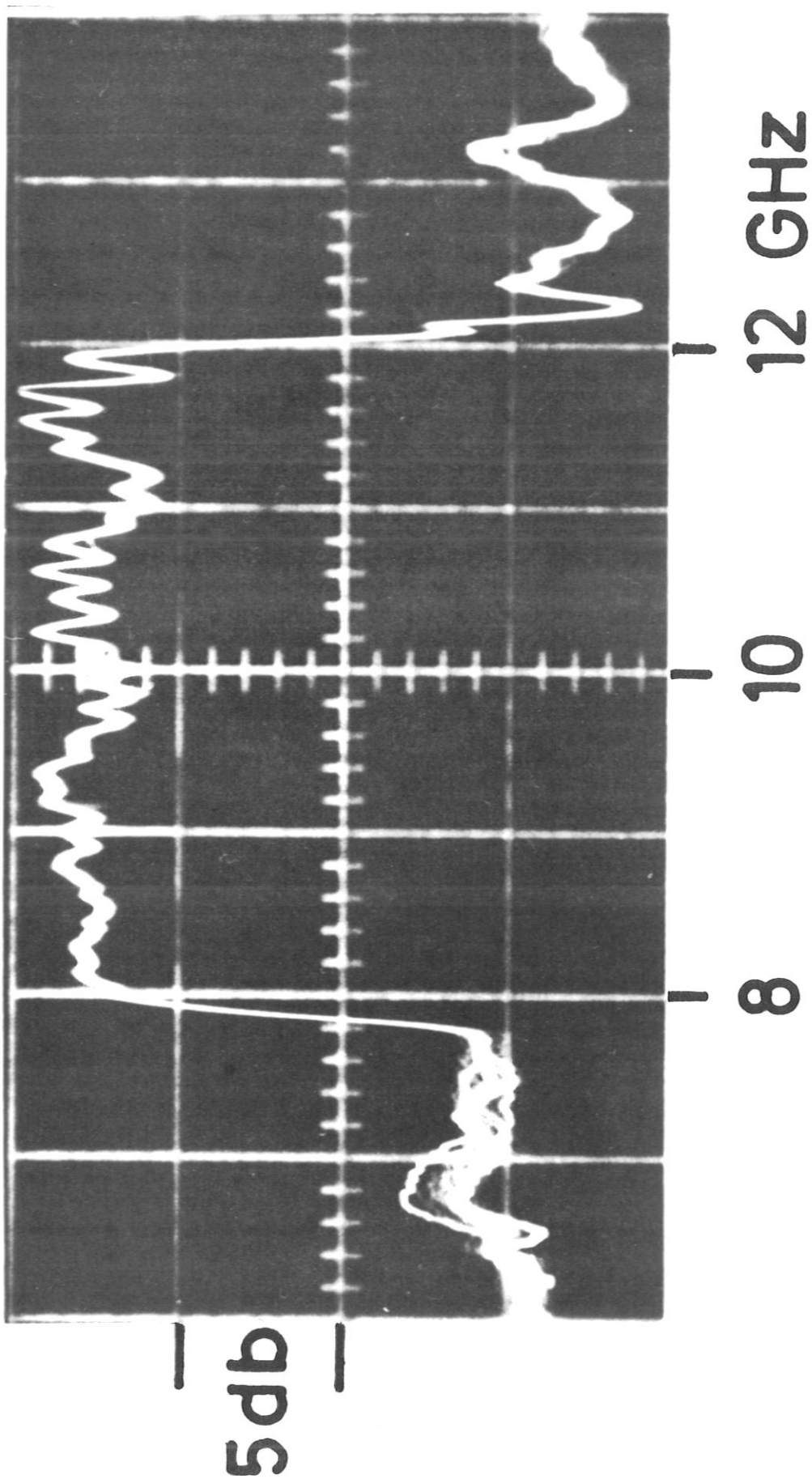

Fig. 2

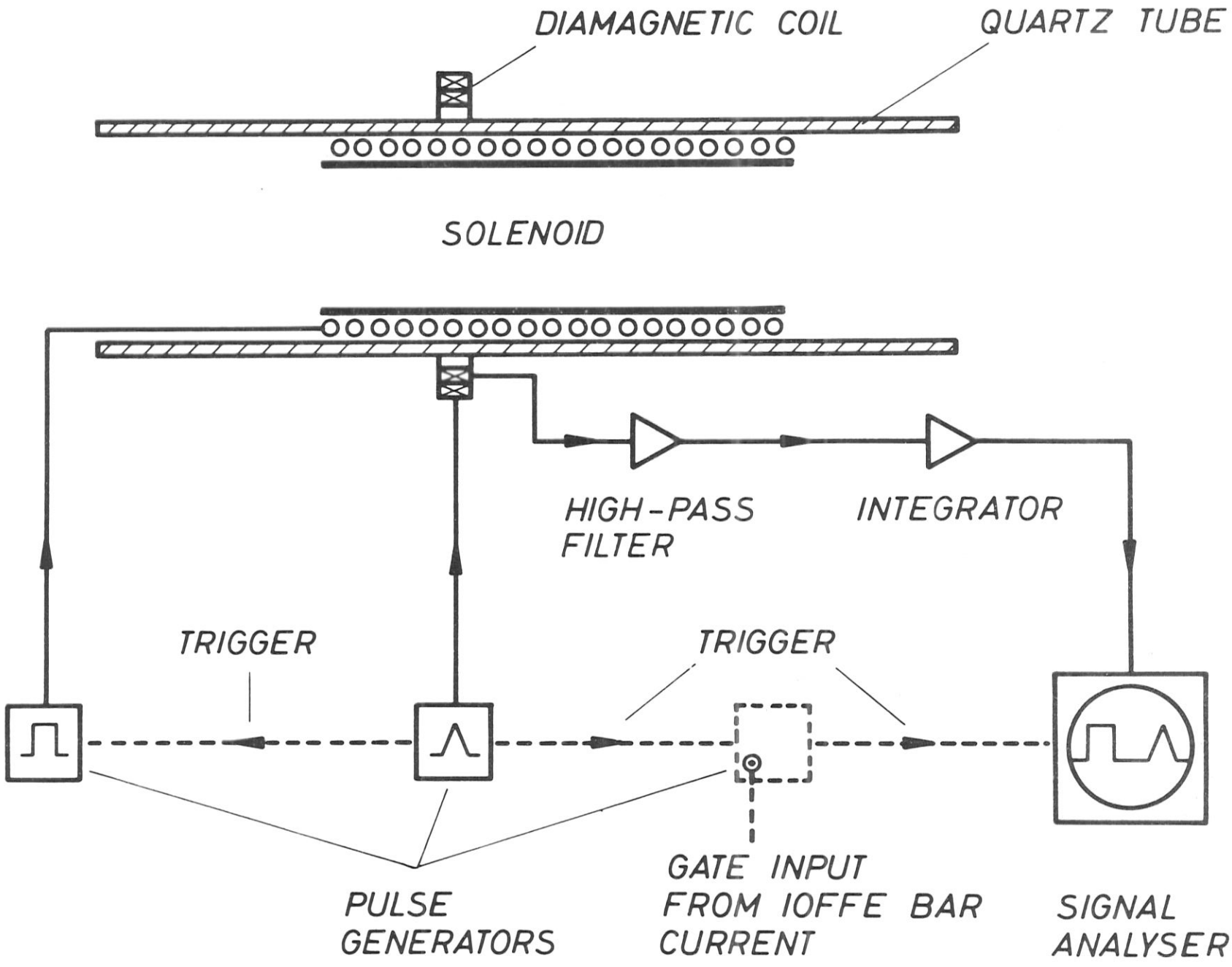
DIAMAGNETIC COIL
QUARTZ TUBE
SOLENOID
HIGH-PASS FILTER
INTEGRATOR
TRIGGER
TRIGGER
PULSE GENERATORS
GATE INPUT FROM IOFFE BAR CURRENT
SIGNAL ANALYSER

Fig. 3

Fig. 4

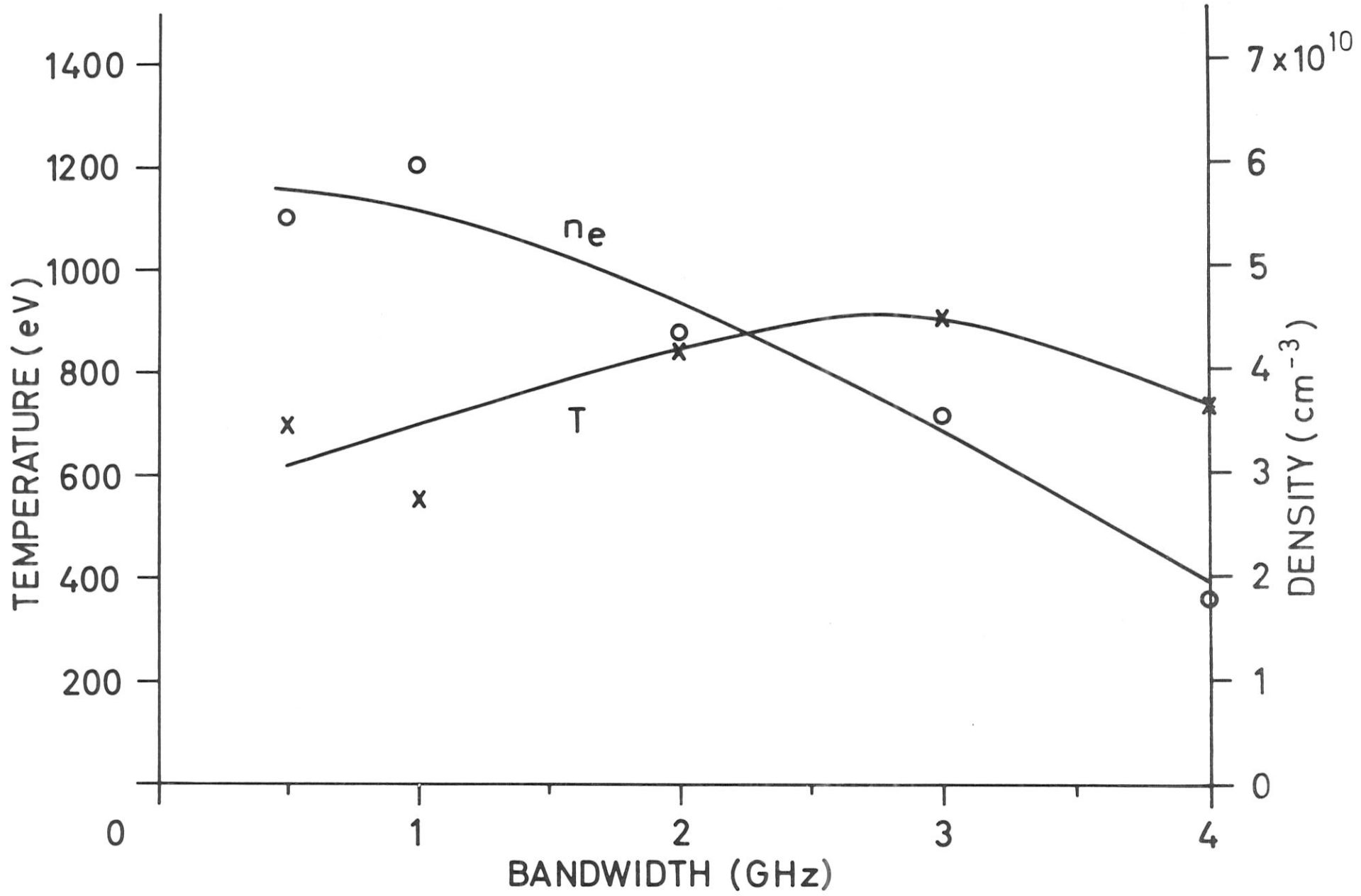
1400
1200
1000
800
600
400
200
0
TEMPERATURE (eV)
7 x 10^10
6
5
4
3
2
1
0
DENSITY (cm^-3)
n_e
T
0
1
2
3
4
BANDWIDTH (GHz)

Fig. 5

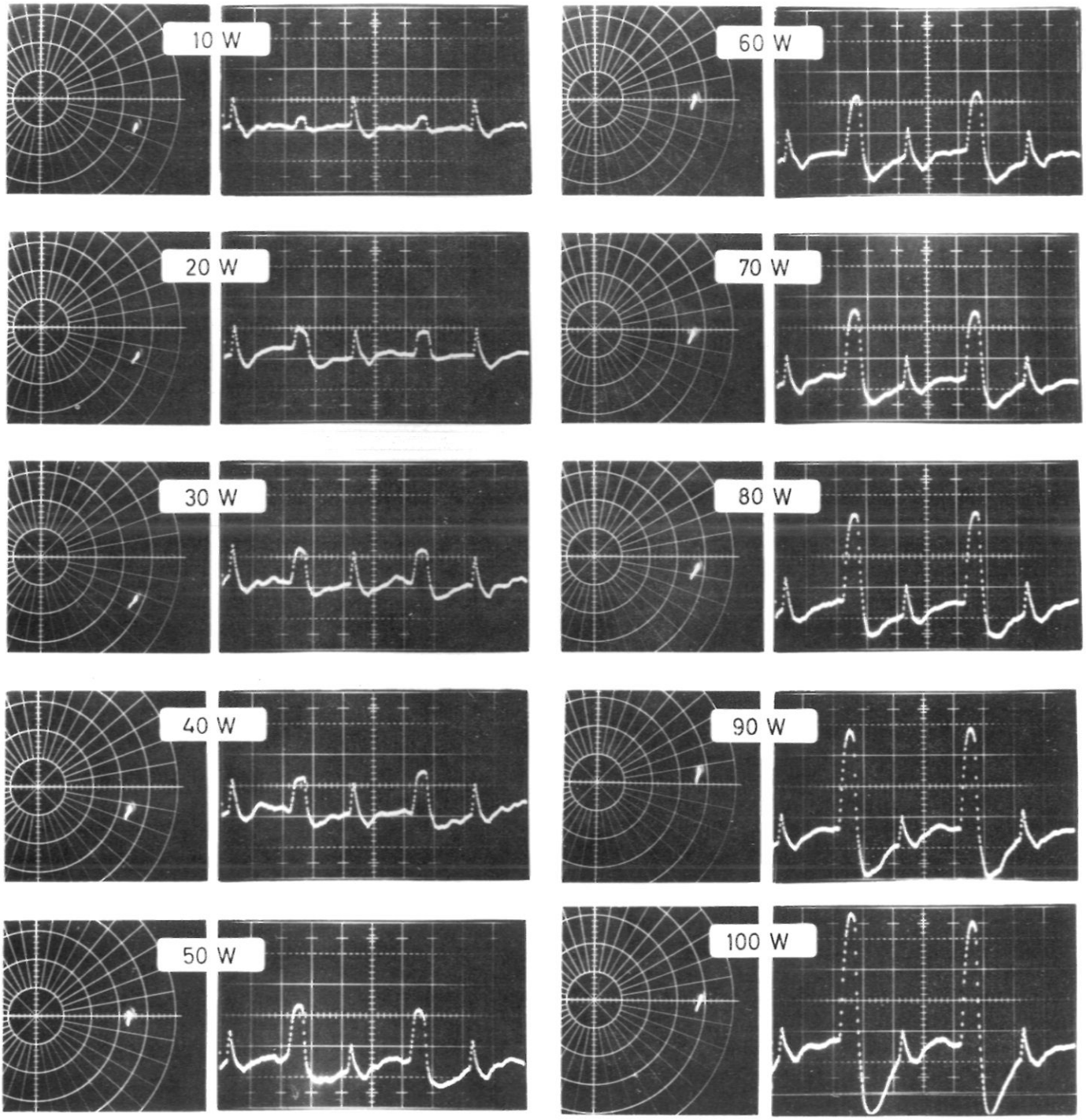

Fig. 6

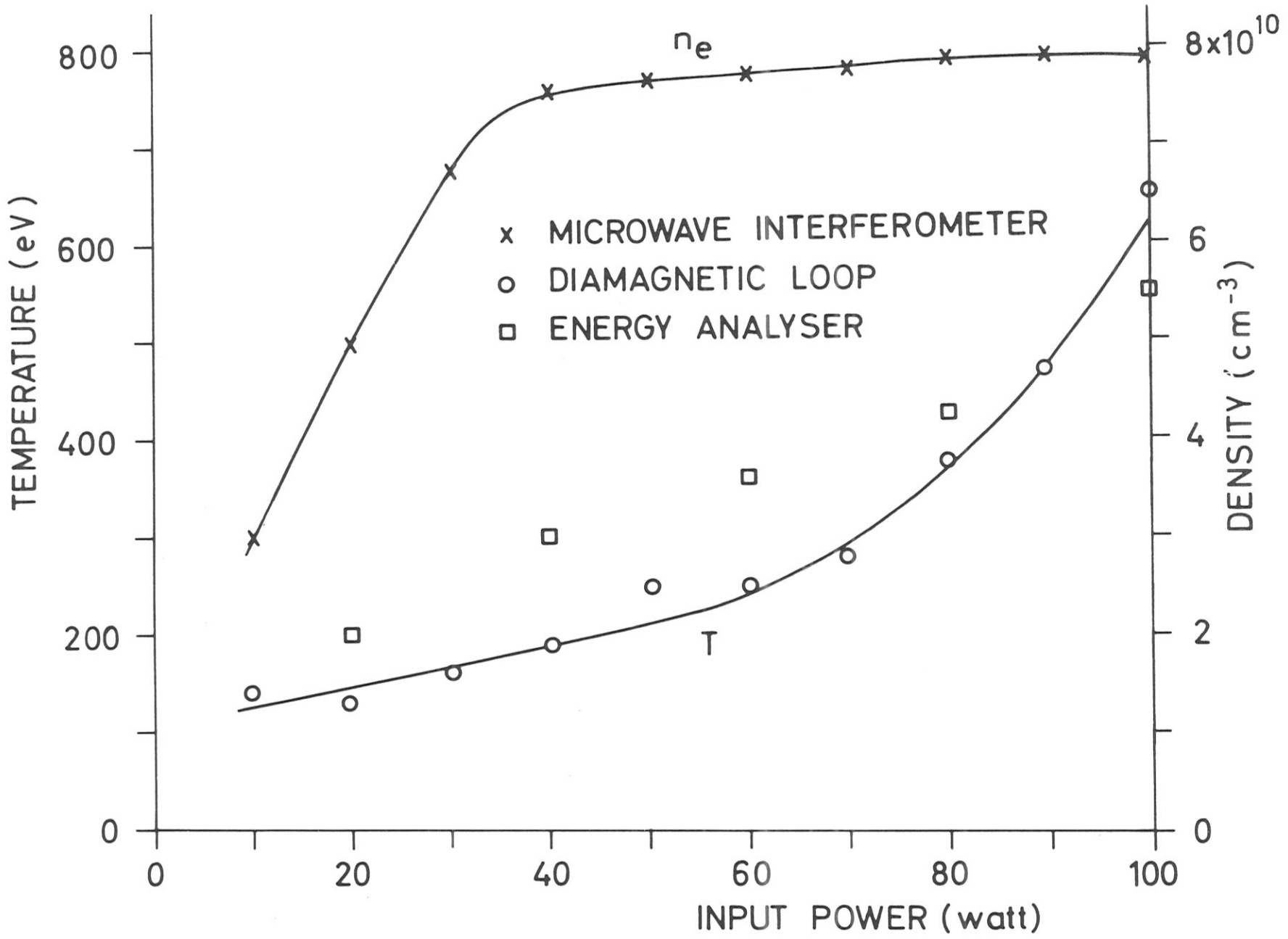
800
600
400
200
0
TEMPERATURE (eV)
n_e
8×10^{10}
6
4
2
0
DENSITY (cm^{-3})
x MICROWAVE INTERFEROMETER
o DIAMAGNETIC LOOP
□ ENERGY ANALYSER
T
0
20
40
60
80
100
INPUT POWER (watt)

Fig. 7

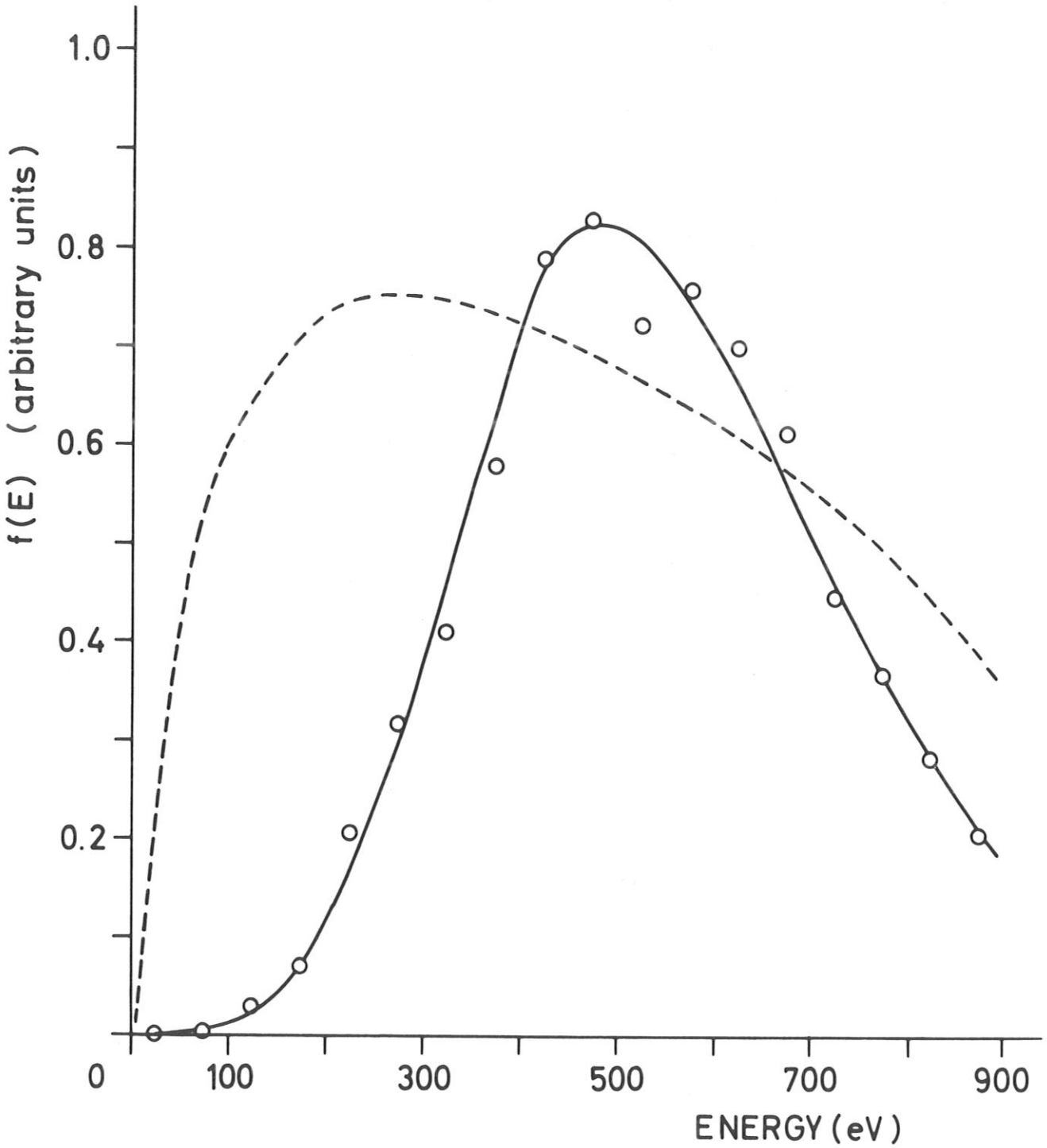
1.0
0.8
0.6
0.4
0.2
0
f(E) (arbitrary units)
100
300
500
700
900
ENERGY (eV)

Fig. 8

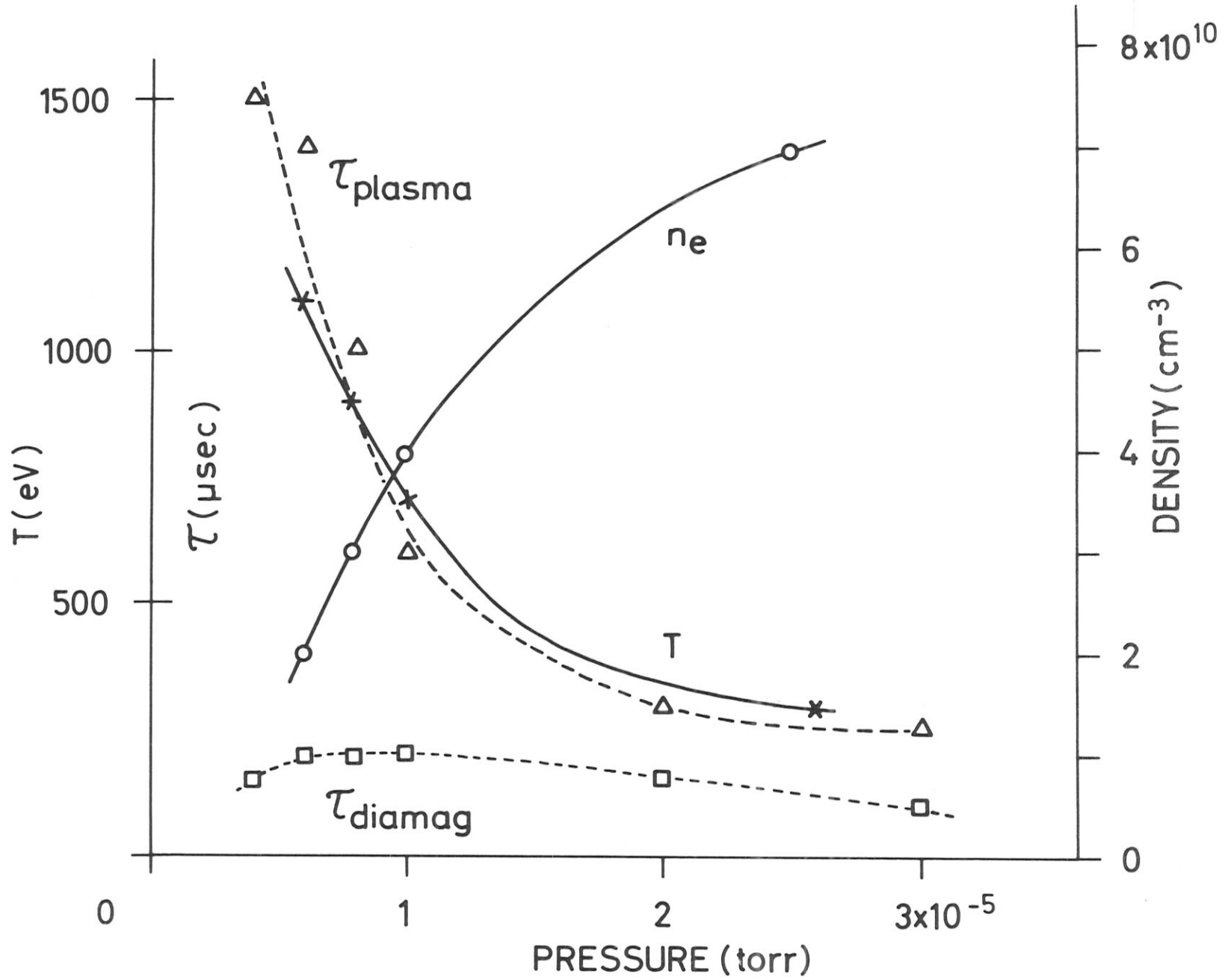
1500
1000
500
0
T (eV)
τ (μsec)
τplasma
ne
T
τdiamag
8x10^10
6
4
2
0
DENSITY (cm^-3)
0
1
2
3x10^-5
PRESSURE (torr)

Fig. 9

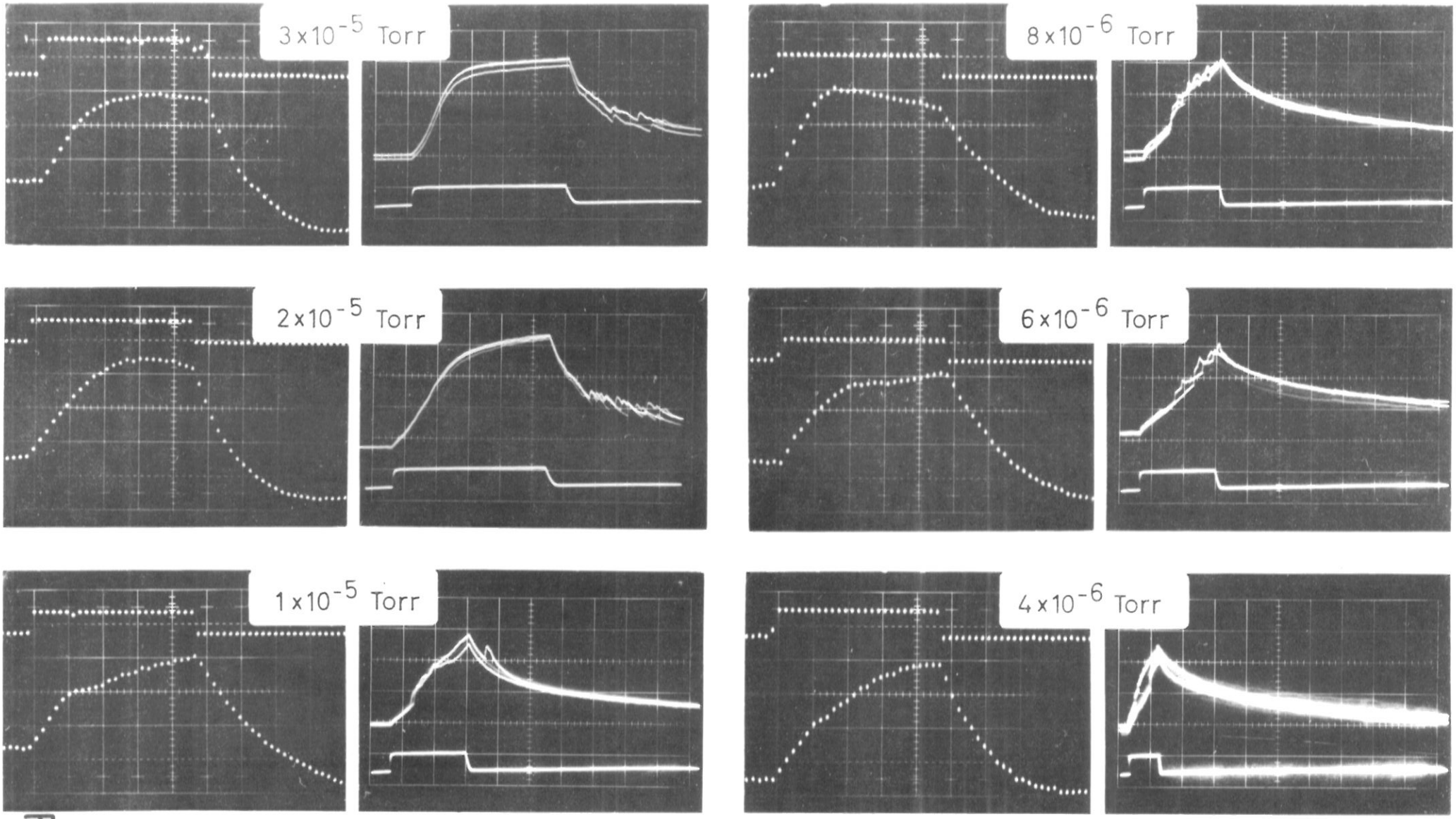
3x10^-5 Torr
8x10^-6 Torr
2x10^-5 Torr
6x10^-6 Torr
1x10^-5 Torr
4x10^-6 Torr

Fig. 10